Research Internship (PRE)

Field of Study: Applied Mathematics
Scholar Year: 2014-2015

Computation of the Effective Dynamic Properties of Composite Materials

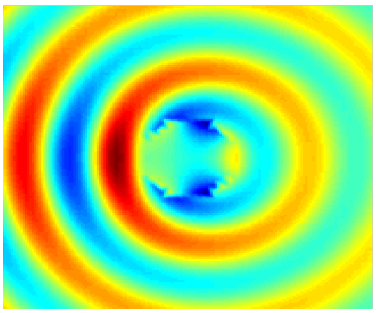

Confidentiality Notice

Non-confidential report and publishable on the Internet

Author:
Rémi FEUILLET

Promotion:
2016

ENSTA ParisTech Tutors:
Sonia FLISS
Stéphanie CHAILLAT

Host Organism Tutor:
Bojan GUZINA

Internship from May 4th 2015 to August 14th 2015

University of Minnesota
Department of Civil,
Environmental and Geo-Engineering
500 Pillsbury Drive S.E
Minneapolis, MN 55455
United States of America

Confidentiality Notice

This present document is not confidential. It can be communicated outside in paper format or distributed in electronic format.

Abstract and Keywords

Composite solids are materials that consist of two or more distinguishable constituents that have different mechanical and physical properties. The composition of these materials (microstructure) can be tailored to provide their better overall performance, characterized by the so-called effective properties. The procedure, in which the effective properties are obtained, is called a homogenization procedure. While numerous reliable homogenization approaches exist for the evaluation of static effective properties, studies of the overall dynamic properties of composites with compact support are still an open question.

The focus of this study is to investigate, implement and develop a computational method for evaluating the effective dynamic properties of composite obstacles. The significant feature of the proposed study is that the effective properties will be obtained using the analysis of far-field behavior of the solutions for various dynamic problems. The approach was first introduced by Maxwell in 1873 in the context of the effective electrical conductivity of materials (static problem). Maxwell suggested that a cluster of representing the material in question affects the fields at large distances from it in the same way as an equivalent sphere whose conductivity is equal to the effective one. However, Maxwell used various simplified assumptions on the geometrical composition of the material and on the shape (spherical) of the equivalent inhomogeneity. The idea of the proposed method is to try to overcome some of these shortcomings and provide accurate estimates of the effective properties for the obstacles with periodic and random structures.

Keywords: Helmholtz Equation, Inverse Problems, Boundary Element Method, Homogenization, Equivalent Inhomogeneity, Polarization Tensor.

Acknowledgment

First, I would like to warmly thank Professor Bojan Guzina for considering and accepting my application as a research intern in the Civil engineering department of the University of Minnesota. As an advisor, his constant support and his large knowledge about the wave propagation were very important to me through all this research project.

Then, I want to express my gratitude to Sonia Fliss, professor and researcher at the ENSTA ParisTech. She helped me finding this high quality internship with a great working environment and I really want to thank her for giving to me that opportunity.

I would like also to thank Stéphanie Chaillat, professor and researcher at the ENSTA ParisTech, who accepted to replace Mrs Fliss for the organization and the examination of my oral defense.

Finally, I also want to thank Fatemeh Pourahmadian, PhD student of the University of Minnesota for having worked with me on this research project. Her relevant piece of advise, especially in mechanics and her daily support were really a benefit for me to pursue in the accomplishment of my research project.

Contents

List of Figures

Introduction

The main study of this internship is the study of dynamic properties of composite materials. Hence, the field of study is between mathematics and mechanics. As student in first year of Master degree in applied mathematics and scientific computing, my competences in the field of mechanics were relatively limited. Therefore, my work as intern in the department of Civil Engineering of the University of Minnesota was more focused on coding and theoretical expectations but in a mathematical way and with limited notions in mechanics.

In this report, my work as intern will be described. In the first part, we will define the physical problem and how to express it formulate it mathematically. Even though this is a shorter part of my report, it is its most significant component since it contains the modeling aspects odf my research.
Then I will show how the problem was implemented using a particular computational technique known as the Boundary Element Method.
Finally, we will see the theoretical considerations concerning the wave propagation in composite materials. These are the so-called transmission problems and we will see how the reasoning has evolved through all the research process, step by step, showing the generalization of the study and the way where the study has gone.

Part 1

Problem Statement

In this internship, the main goal is the study the effective elastic properties of composite materials. For that purpose, some simulations are needed to illustrate theoretical considerations. The idea of the homogenization procedure is to see to which extent a ser of inclusions in a given material can have the same far field pattern as an equivalent inhomogeneity (e.g. a circle). Since we are dealing with the case of elastic waves, two point of view have been used : the point of view of acoustics and then the point of view of elastodynamics with viscoelastic SH-waves, which can be considered to some extent as a generalization of the first case. In both cases, we are considering the following transmission problem with the Sommerfeld radiation condition:

$$\begin{cases} \Delta u^s + k^2 u^s = 0 \text{ in } \mathbb{R}^2 \setminus \Omega \\ \Delta u^t + \gamma^2 k^2 u^t = 0 \text{ in } \Omega \\ \lim\limits_{|x|\to\infty} |x| \left\{ \dfrac{\partial}{\partial |x|} - ik \right\} u^s(x) = 0 \end{cases}$$

The following relations and boundary conditions are satisfied:

$$\begin{cases} u^{inc}(x) = e^{ikx.\vec{d}} \text{ where } \vec{d} \text{ is an unit vector} \\ u^t = u^s + u^{inc} \text{ in } \mathbb{R}^2 \setminus \bar{\Omega} \\ u^t(x) = u^s(x) + u^{inc}(x) \text{ for } x \in \partial\Omega \\ \beta u^t_{,n}(x) = u^s_{,n}(x) + u^{inc}_{,n}(x) \text{ for } x \in \partial\Omega \end{cases}$$

where u^s represents the scattered field created by the inhomogeneity thanks to the incident wave represented by u^{inc}, which is the free field solution and consequently, u^t is the total field.
Note that k is the wave number, γ is the contrast and represents the difference between the two materials. β is the transmission coefficient. If $\beta = 0$, it is a Neumann problem and if $\beta = +\infty$, it is a Dirichlet problem. These two coefficients can be either real (case of acoustics) or complex (viscoelastic waves).

Part 2

Implementation of the Code

2.1 The Boundary Element Method

In order to simulate our waves we use the Boundary Element Method. This method is well explained in [1]. We will only see a simplified version.
First, this method relies on the Boundary Integral Equations :

2.1.1 The Boundary Integral Equations

Let us consider a bounded domain $\Omega \subset \mathbb{R}^2$ and a second order differential partial equation :

$$\mathcal{L}u = 0 \text{ in } \Omega$$

with suitable boundary conditions on $\partial\Omega$. Let us denote the Green function $G(x, y)$ as the solution to the equation $\mathcal{L}u + \delta(y - x) = 0$ and let $H(x, y)$ denote its normal derivative. Then if q is the normal derivative of u, the following formulas for the interior problem (e.g $\mathcal{L}u = 0$ in Ω) are obtained (They are proved in [1] as long as $\partial\Omega$ is smooth at x):

$$\begin{cases} u(x) = \int\limits_{\partial\Omega} q(y)G(x,y) - u(y)H(x,y)\mathrm{d}\Gamma_y \text{ for } x \in \Omega \\ \frac{1}{2}u(x) = \int\limits_{\partial\Omega} q(y)G(x,y) - u(y)H(x,y)\mathrm{d}\Gamma_y \text{ for } x \in \partial\Omega \\ 0 = \int\limits_{\partial\Omega} q(y)G(x,y) - u(y)H(x,y)\mathrm{d}\Gamma_y \text{ for } x \in \mathbb{R}^2 \setminus \Omega \end{cases}$$

Actually, these equalities remain identical for the exterior problem (e.g $\mathcal{L}u = 0$ in $\mathbb{R}^2 \setminus \Omega$) as long as the normal to $\partial\Omega$ is changed to his opposite in both G and q.
Now, let us consider the particular case of $\mathcal{L}$, that is to say our set of equations for the Helmholtz transmission problem: $\mathcal{L} = \Delta + k^2 I$ and $\mathcal{L} = \Delta + \gamma^2 k^2 I$.
The associated Green function is :

$$\begin{cases} G(x, y; k) = \frac{i}{4} H_0^1(k|x - y|) \text{ if } k \neq 0 \\ G(x, y; 0) = -\frac{1}{2\pi} \ln(|x - y|) \end{cases}$$

where H_m^1 is the Hankel function of first kind and order m.
If we consider the normal derivative after $\vec{n}$, which is the outer normal to $\partial\Omega$, we can obtain with the same notations as previously and $x \in \partial\Omega$.

$$\begin{cases} \frac{1}{2}u^s(x) = \int_{\partial\Omega} (-u^s_{,n})(y)G(x,y;k) - u^s(y)(-H(x,y;k))\mathrm{d}\Gamma_y \\ \frac{1}{2}u^s(x) = -\frac{1}{2}u^{inc}(x) + \int_{\partial\Omega} \frac{1}{\beta}(u^s_{,n}(y) + u^{inc}_{,n}(y))G(x,y;\gamma k) - (u^s(y) + u^{inc}(y))(H(x,y;\gamma k))\mathrm{d}\Gamma_y \end{cases}$$

It is important to notice that first, these integrals are weekly singulars because both G and H are singular when $x = y$ and then, that the boundary conditions are used for the second equation.

2.1.2 Discretization

The integral equations are now obtained and the next step is to discretize them in order to compute numerically u^s on the boundary and then at any point of point inside the domain.
The discretization process is divided in several steps. First, a discretization of the boundary is made and then the unknown are discretized to finally obtain a linear system of equations.

Discretization of the Boundary

In this part, we consider a partition of N_E non-intersecting smaller elements called Boundary Elements denoted E_e (for $e \in [|1, N_E|]$) whose union gives a good approximation of the boundary $\partial\Omega$. In our 2D-case, the elements will be simple segments. Consequently, our integral on $\partial\Omega$ can be replaced by the sum of the integrals on E_e.
Now, we need to establish a mapping of each element. For that purpose, nodes and shape functions are needed. Each element E_e is mapped onto a real segment I using the following formula:

$$y(\xi) = \sum_{i=1}^{3} N_i(\xi) y^i \text{ for } \xi \in I$$

where y^i are the nodes (so-called collocation points), y is the coordinates of a point in E_e and N_i are the shape functions given by:

$$\begin{cases} N_1(\xi) = \frac{1}{2}\xi(\xi - 1) \\ N_2(\xi) = 1 - \xi^2 \\ N_3(\xi) = \frac{1}{2}\xi(\xi + 1) \end{cases}$$

If we denote ξ^i the antecedent of y^i, we can notice that the shape functions satisfy the following relationship :

$$N_j(\xi^i) = \delta_{i,j} \text{ and } \sum_{i=1}^{3} N_i(\xi) = 1 \ \forall \xi \in I$$

In order to obtain a linear mapping in ξ, y^2 is chosen as the middle of y^1 and y^3 so that the quadratic term in ξ vanishes. Moreover, for this particular case, we can express both the unit normal and the differential element as:

$$\mathrm{d}\Gamma = |\sum_{i=1}^{3} N'_i(\xi)| d\xi \text{ and } n = \frac{1}{|y^3 - y^1|}(-(y^3 - y^1).e_y, (y^3 - y^1).e_x)$$

Discretization of the Unknowns

The next step is the discretization of the unknowns u and $u_{,}n$. For that purpose, an interpolation technique is used. In our specific case, the interpolation nodes y^i are the same as the collocation points and the interpolation functions are the shape functions (isoparametrical interpolation). Consequently, we obtain the following approximations of u and $u_{,n}$:

$$\tilde{u}(y) = \sum_{i=1}^{3} N_i(\xi) u(y^i) \text{ and } \tilde{u_{,n}}(y) = \sum_{i=1}^{3} N_i(\xi) u_{,n}(y^i)$$

Discretized Equation

The last step required to finally obtain the discretization of our equation is to evaluate this equation for each collocation point, in other words to take $x = y^i$ where $i = 1, 2, 3$ in the local numbering of each element. Consequently, we obtain $3N_E$ set of 2 equations of the kind (for $m \in [|1; N_E|]$, i.e in global numbering):

$$\begin{cases} \frac{1}{2}u^s(y^m) = \sum_{e=1}^{N_E} \sum_{i(e)=1}^{3} -u^s_{,n}(y^{i(e)}) \int_{E_e} N_{i(e)}(\xi) G(y^m, y(\xi); k) \mathrm{d}\Gamma(\xi) \\ \qquad\qquad - \sum_{e=1}^{N_E} \sum_{i(e)=1}^{3} u^s(y^{i(e)}) \int_{E_e} N_{i(e)}(\xi)(-H(y^m, y(\xi); k)) \mathrm{d}\Gamma(\xi) \\ \\ \frac{1}{2}u^s(y^m) = -\frac{1}{2}u^{inc}(y^m) + \sum_{e=1}^{N_E} \sum_{i(e)=1}^{3} (u^s_{,n}(y^{i(e)}) + u^{inc}_{,n}(y^{i(e)})) \int_{E_e} N_{i(e)}(\xi) G(y^m, y(\xi); \gamma k) \mathrm{d}\Gamma(\xi) \\ \qquad\qquad - \sum_{e=1}^{N_E} \sum_{i(e)=1}^{3} (u^s(y^{i(e)}) + u^{inc}(y^{i(e)})) \int_{E_e} N_{i(e)}(\xi)(H(y^m, y(\xi); \gamma k)) \mathrm{d}\Gamma(\xi) \end{cases}$$

These equations can be put into a matrix form:

$$\begin{pmatrix} A & B \\ C & D \end{pmatrix} \begin{pmatrix} X \\ Y \end{pmatrix} = \begin{pmatrix} E \\ F \end{pmatrix}$$

where A, B, C, D are matrices of size $3N_E \times 3N_E$, X, Y, E, F are matrices of size $3N_E \times 1$ and are defined by :

$$\begin{cases} A_{ij} = \frac{1}{2}\delta_{ij} + \int\limits_{E_e} N_{j'}(\xi)(-H(y^i, y(\xi); k))\mathrm{d}\Gamma(\xi) \\ B_{ij} = \int\limits_{E_e} N_{j'}(\xi)(G(y^i, y(\xi); k))\mathrm{d}\Gamma(\xi) \\ C_{ij} = \frac{1}{2}\delta_{ij} + \int\limits_{E_e} N_{j'}(\xi)(H(y^i, y(\xi); \gamma k))\mathrm{d}\Gamma(\xi) \\ D_{ij} = -\int\limits_{E_e} N_{j'}(\xi)(G(y^i, y(\xi); \gamma k))\mathrm{d}\Gamma(\xi) \\ X_i = u^s(y^i) \\ Y_i = u^s_{,n}(y^i) \\ E_i = 0 \\ F_i = -\frac{1}{2}u^{inc}(y^i) + \sum\limits_{e=1}^{N_E}\sum\limits_{j(e)=1}^{3}(u^{inc}_{,n}(y^{j(e)}))\int\limits_{E_e} N_{j(e)}(\xi)G(y^i, y(\xi); \gamma k)\mathrm{d}\Gamma(\xi) \\ \qquad -\sum\limits_{e=1}^{N_E}\sum\limits_{j(e)=1}^{3}(u^{inc}(y^{j(e)}))\int\limits_{E_e} N_{j(e)}(\xi)(H(y^i, y(\xi); \gamma k))\mathrm{d}\Gamma(\xi) \end{cases}$$

In all these equations, $i, j \in [|1; 3N_E|]$, $j' = j\ mod(3) + 3$ (j' is the local numbering) and E_e is the element in which y^i belongs.

2.1.3 Implementation

To implement this method, MatLab software is used. The main steps of the code are explained in this part. First of all, it is needed to define numerically the position of the collocation points on each element. As previously stated, three points are chosen so that one is the middle point between the two others. Moreover the two other points are chosen inside the element in order to avoid singularities on the boundary of each element.
These points are defined by three parameters LK, $LR > LK$ and $Mi = \frac{LR}{2}$. Therefore, if we denote z_{beg} and z_{end} the extreme points of the element, we can define the coordinates of the collocation points and the bounds ξ_{min} and ξ_{max} for the parameter ξ :

$$\begin{cases} y^1 = z_{beg} + \frac{LK}{LR}(z_{end} - z_{beg}) \\ y^2 = z_{beg} + \frac{Mi}{LR}(z_{end} - z_{beg}) \\ y^3 = z_{beg} + \frac{LR - LK}{LR}(z_{end} - z_{beg}) \\ \xi_{min} = -\frac{LR}{2LK - LR} \\ \xi_{max} = \frac{LR}{2LK - LR} \end{cases}$$

For all computations, we take $LK = 3$ and $LR = 4$

Then, since MatLab is used for numerical computations, we have to take care of some particular cases :

- The case $k = 0$ and/or $\gamma = 0$: the Green function and its derivative need to be replaced by $G(x, y; 0)$ and its derivative in the code.
- The case when the Green functions and its derivative are singular inside the integration domain. The integral remains evaluated though, but MatLab is unable to notice the singularity. Consequently we need, for that case, to replace $G(x, y; k)$ by $G(x, y; k) - G(x, y; 0)$ which is non singular and its derivative neither (see [1]) and to write the exact formula obtained with $G(x, y; 0)$ (static case) thanks to Mathematica via Cauchy principal value computation formula (where ξ_{sing} is the interior point in which the integrated function is singular):

$$\text{p.v.}(\int_{\xi_{min}}^{\xi_{max}} f(\xi)d\xi) = \lim_{h\to 0}(\int_{\xi_{min}}^{\xi_{sing}-h} f(\xi)d\xi + \int_{\xi_{sing}+h}^{\xi_{max}} f(\xi)d\xi)$$

Finally, here is the description of Boundary Element Method MatLab script in pseudo code:

```
Input : k, beta, gamma, d, type of geometry, number of
   elements

Discretization of the geometry and creation of elements
   and collocation points
For each element
 Consider one collocation point
  Another loop on all elements
   if collocation point is in the element then give
      Mathematica formula for static integral and replace
       Green function by its difference with static one
   if k=0 or/and gamma=0 then choose the related Green
      function
   Computing all the integrals for both problems
   Fill in matrices for both right and left hand sides
Solve linear system

Output: u and its normal derivative evaluated in the
   collocation points
```

2.1.4 Computation of the Field

Thanks to the previous script,the value of u^s in all the collocation points on the boundary can be computed.
Now, the next step is to compute the field inside and outside the inhomogeneity. In the same way as the previous case, we use boundary integral equations to compute this field:

$$\begin{cases} u^s(x) = \int\limits_{\partial\Omega} (-u^s_{,n})(y)G(x,y;k) - u^s(y)(-H(x,y;k))\mathrm{d}\Gamma_y \ \forall x \in \mathbb{R}^2 \setminus \bar{\Omega} \\ u^t(x) = \int\limits_{\partial\Omega} \frac{1}{\beta}(u^s_{,n}(y) + u^{inc}_{,n}(y))G(x,y;\gamma k) - (u^s(y) + u^{inc}(y))(H(x,y;\gamma k))\mathrm{d}\Gamma_y \ \forall x \in \Omega \end{cases}$$

Which leads us to the following discretized equation for $x \in \mathbb{R}^2 \setminus \bar{\Omega}$:

$$\begin{aligned} u^s(x) = &\sum_{e=1}^{N_E} \sum_{i(e)=1}^{3} -u^s_{,n}(y^{i(e)}) \int\limits_{E_e} N_{i(e)}(\xi)G(x,y(\xi);k)\mathrm{d}\Gamma(\xi) \\ &- \sum_{e=1}^{N_E} \sum_{i(e)=1}^{3} u^s(y^{i(e)}) \int\limits_{E_e} N_{i(e)}(\xi)(-H(x,y(\xi);k))\mathrm{d}\Gamma(\xi) \end{aligned}$$

and for $x \in \Omega$:

$$\begin{aligned} u^t(x) = &\sum_{e=1}^{N_E} \sum_{i(e)=1}^{3} (u^s_{,n}(y^{i(e)}) + u^{inc}_{,n}(y^{i(e)})) \int\limits_{E_e} N_{i(e)}(\xi)G(x,y(\xi);\gamma k)\mathrm{d}\Gamma(\xi) \\ &- \sum_{e=1}^{N_E} \sum_{i(e)=1}^{3} (u^s(y^{i(e)}) + u^{inc}(y^{i(e)})) \int\limits_{E_e} N_{i(e)}(\xi)(H(x,y(\xi);\gamma k))\mathrm{d}\Gamma(\xi) \end{aligned}$$

It is important to notice that in these cases, we do not have to cope anymore with the case of singular integrals since $x \notin \partial\Omega$.

2.1.5 Generalization to Multiple Inclusions

In all the previous part, the only assumption made on Ω is that it is a bounded domain. Consequently, the following formulas can be used with multiple inclusions. Moreover, we can notice that if γ is constant of value γ_k inside each inclusion, the boundary integral stay the same as long as the Green function is changed for the interior problem. Consequently, our set of equations is the following for $x \in \partial\Omega$:

$$\begin{cases} \frac{1}{2}u^s(x) = \int\limits_{\partial\Omega} (-u^s_{,n})(y)G(x,y;k) - u^s(y)(-H(x,y;k))\mathrm{d}\Gamma_y \\ \frac{1}{2}u^s(x) = -\frac{1}{2}u^{inc}(x) + \sum\limits_{k=1}^{N_{inhom}} \int\limits_{\partial\Omega_k} \frac{1}{\beta}(u^s_{,n}(y) + u^{inc}_{,n}(y))G(x,y;\gamma(x)k) \\ \qquad\qquad - \sum\limits_{k=1}^{N_{inhom}} \int\limits_{\partial\Omega_k} (u^s(y) + u^{inc}(y))(H(x,y;\gamma(x)k))\mathrm{d}\Gamma_y \end{cases}$$

with the following notations: $\Omega = \bigcup\limits_{k=0}^{N_{inhom}} \Omega_k$ and $\gamma(x) = \gamma_k$ if $x \in \Omega_k$ Then, the process is exactly the same as explained previously with one inclusion

2.2 Other Functions

Computation of the Boundary Integral

Since we have the coordinates of the collocation points and the shape functions, we can easily compute the integral of u^t or any other quantity as long as its value in the

collocation points is known. All relies on the following formula :

$$\int_{\partial\Omega} f(y)\mathrm{d}\Gamma_y = \sum_{e=1}^{N_E} \sum_{i(e)=1}^{3} \int_{E_e} N_{i(e)} f(y^{i(e)})(\xi)\mathrm{d}\Gamma(\xi)$$

Computation of a Surface Integral

As we will see later, it is needed for theoretical reasons to compute the integral of u^t inside each inhomogeneity. Since it is a surface integral, there are not simple MatLab functions planned for that case. That is why a simple numerical method was implemented since most of the computations were made with highly symmetric shaped inhomogeneities. Basically, the geometries used in most of the cases are regular polygons constructed thanks to a circle. Consequently, one way to discretize the inhomogeneity, is to consider a smaller circle and then generate the smaller polygon associated. In the space between these two polygons, small trapezes can be generated. The process continues until the center of all circles is reached (in the last level, triangles are generated). The next step consists to compute the value of u^t in the middle of each small element and to multiply it by the area of the element. The sum gives us an approximation of the integral of u^t over the inhomogeneity.

2.3 Adaptation for a Static Problem

In order to double check some results obtained in a static study, I was asked to adapt this code for the following static problem:

$$\begin{cases} \Delta u = 0 \text{ in } \mathbb{R}^2 \setminus \Omega \\ \Delta u = 0 \text{ in } \Omega \\ u(x_-) = u(x_+) \text{ in } \partial\Omega \\ K\dfrac{\partial u}{\partial n}(x_-) = \dfrac{\partial u}{\partial n}(x_+) \text{ in } \partial\Omega \\ \lim\limits_{|x|\to\infty} \dfrac{\partial u}{\partial x} = 1 \end{cases}$$

If we use the following change of variable in $\mathbb{R}^2 \setminus \Omega$: $u_1(x,y) = u(x,y) + x$, then u_1 still satisfies the Laplace equation, and the equations are transformed as:

$$\begin{cases} u(x_-) = u_1(x_+) + x \text{ in } \partial\Omega \\ K\dfrac{\partial u}{\partial n}(x_-) = \dfrac{\partial}{\partial n}(u_1(x_+) + x) \text{ in } \partial\Omega \\ \lim\limits_{|x|\to\infty} \dfrac{\partial u_1}{\partial x} = 0 \end{cases}$$

Consequently, if k is set to 0, and u^{inc} is replaced by x, the problem is the same as ours and the code can be used for this static study.
The output to be computed is (u is real):

$$\oint_\Omega u\mathrm{d}z = \oint_\Omega u\mathrm{d}x + i\{\oint_\Omega u\mathrm{d}y\}$$

It can be computed via a parameterization of x and y and then our function which computes boundary integrals.
Results obtained via this code are apparently better than results obtained via the other even if computation process is longer.

2.4 Comments about the Code

This code has been implemented first to confirm theoretical results (and validated by these same studies) and then to test some unknowns cases so that we can find an equivalent inhomogeneity thanks to theoretical studies.
On a more technical point of view, the code was used most of the time with a discretization of near 50 elements so that computation time was reasonable (nearly 150s for the boundary element method), since the algorithm has a quadratic complexity in the number of elements. Furthermore, and on the contrary to finite elements, matrices used in this code are neither symmetric nor empty, which means that for the same level of discretization, the method will be longer with a BEM than with a FEM.
The implementation of this code was not so easy since I had to start from the scratch in everything : I did not know anything about neither homogenization nor Boundary Element Method. The mathematical modelling even if really nice and interesting is sometimes difficult to be understood and implemented with MatLab. Moreover, it is really important to be cautious about what we want to compute. In the first reading of the theoretical part of our transmission problem, I thought we had to compute the integral on the boundary instead of the surface integral. This mistake was revealed after a week of simulations, that is a bit tough ....
Nonetheless, this coding part which took place during the first half of my internship, was really interesting.

Part 3

Theoretical Study

3.1 Transmission Problem Generalities

Now, our main goal is to focus on the study of the far-field pattern generated by a circle and more generally by any inclusion or a bunch of inclusions.
As viewed in the previous part, we can formulate $u^s(x)$ for $x \in \mathbb{R} \setminus \Omega$ as the following boundary integral:

$$u^s(x) = \int_{\partial\Omega} u^s_{,n}(y)G(x,y;k) - u^s(y)G_{,n}(x,y;k)\mathrm{d}\Gamma_y$$

where $G(x,y;k)$ is the Green function from the previous part and n the inner normal to the inhomogeneity. Moreover, since u^i satisfies the Helmholtz equation with k as parameter in Ω, we have with the same normal n:

$$0 = \int_{\partial\Omega} (-u^i_{,n}(y))G(x,y;k) - u^i(y)(-G_{,n}(x,y;k))\mathrm{d}\Gamma_y$$

Therefore, it can be shown that:

$$u^s(x) = \int_{\partial\Omega} \beta u^t_{,n}(y)G(x,y;k) - u^t(y)G_{,n}(x,y;k)\mathrm{d}\Gamma_y$$

Based on the expansions of the Hankel function given in [2], we have for large values of x (with $\hat{x}$ as its unit direction) :

$$G(x,y;k) = \frac{i}{4}H_0^1(k|x-y|) \underset{|x|\to\infty}{\sim} \frac{i}{4}\sqrt{\frac{2}{\pi}}e^{\frac{-i\pi}{4}}\frac{e^{ik|x|}}{\sqrt{k|x|}}e^{-ik\hat{x}.y}$$

Hence we find the expression:

$$u^s(x) \underset{|x|\to\infty}{\sim} \frac{e^{ik|x|}}{\sqrt{k|x|}}\frac{i}{4}\sqrt{\frac{2}{\pi}}e^{\frac{-i\pi}{4}}u^s_\infty(\hat{x})$$

with:

$$u^s_\infty(\hat{x}) = \int_{\partial\Omega} \beta u^t_{,n}(y)e^{-ik\hat{x}.y} - u^t(y)\frac{\partial}{\partial n(y)}(e^{-ik\hat{x}.y})\mathrm{d}\Gamma_y$$

3.2 Transmission Problem with $\beta = 1$

Now let us simplify the previous expression when $\beta = 1$, set $\omega = e^{-ik\hat{x}.y}$ and thanks to the following set of equations in Ω, we have:

$$\begin{cases} \Delta\omega + k^2\omega = 0 \\ \Delta u^t + \gamma^2 k^2 u^t = 0 \end{cases} \iff \begin{cases} \int\limits_\Omega \Delta\omega u^t + k^2\omega u^t \mathrm{d}S_y = 0 \\ \int\limits_\Omega \Delta u^t \omega + \gamma^2 k^2 \omega u^t \mathrm{d}S_y = 0 \end{cases}$$

By applying Green formulas and using $\beta = 1$, we can obtain:

$$\begin{cases} -\int\limits_{\partial\Omega} \frac{\partial\omega}{\partial n(y)} u^t \mathrm{d}\Gamma_y - \int\limits_\Omega \nabla u^t.\nabla\omega \mathrm{d}S_y + k^2 \int\limits_\Omega \omega u^t \mathrm{d}S_y = 0 \\ -\int\limits_{\partial\Omega} u^t_{,n}\omega \mathrm{d}\Gamma_y - \int\limits_\Omega \nabla u^t.\nabla\omega \mathrm{d}S_y + \gamma^2 k^2 \int\limits_\Omega \omega u^t \mathrm{d}S_y = 0 \end{cases}$$

so that

$$u^s_\infty(\hat{x}) = -k^2(1-\gamma^2) \int\limits_\Omega u^t e^{-ik\hat{x}.y} \mathrm{d}S_y$$

3.2.1 Case of a Single Circle

In the case of one circle of radius R (Ω here), the exact formula is well known (e.g in [3]), thus for $x \in \mathbb{R}^2$:

$$u^s(x) = \sum_{n=0}^{\infty} A^*_n H^1_n(k|x|)\cos(n(\theta - \alpha))$$

with:

$$\begin{cases} \theta = arg(x) \\ \alpha = arg(\vec{d}) \\ A^*_n = ((-i)^n \epsilon_n) \dfrac{\gamma J_n(kR) J'_n(\gamma kR) - J'_n(kR) J_n(\gamma kR)}{\gamma H^1_n(kR) J'_n(\gamma kR) - H^{1\prime}_n(kR) J_n(\gamma kR)} \\ \epsilon_0 = 1 \\ \epsilon_{\geq 1} = 2 \end{cases}$$

Where J_n is the Bessel Function of first kind.
Now, thanks to [2], we have the following expansion:

$$H^1_n(k|x|) \underset{|x|\to\infty}{\sim} \sqrt{\frac{2}{\pi k|x|}} e^{i(k|x| - \frac{\pi}{4} - n\frac{\pi}{2})}$$

which gives us the final formula:

$$u^s_\infty(\hat{x}) = \sum_{n=0}^{\infty} -4iA^*_n e^{-in\frac{\pi}{2}} \cos(n(\theta - \alpha))$$

Now, let us obtain other interesting properties related to u. First, thanks to Jacobi-Anger expansion :

$$e^{-ik\hat{x}.y} = e^{-ik|y|\cos(\theta - \lambda(y))} = \sum_{n=-\infty}^{+\infty} (-i)^n J_n(k|y|) e^{-in(\theta - \lambda(y))}$$

Hence, the following expression, can be obtained since Ω is considered as a smooth enough bounded domain:

$$-k^2(1-\gamma^2)\sum_{n=-\infty}^{+\infty}(-i)^n\int_\Omega u^t(y)J_n(k|y|)e^{in\lambda(y)}\mathrm{d}S_y e^{-in\theta}=\sum_{n=-\infty}^{+\infty}-\frac{4}{\epsilon_{|n|}}iA_n^*e^{-in\frac{\pi}{2}}e^{-in\alpha}e^{in\theta}$$

Which means by uniqueness of Fourier series expansion that$(n=0)$:

$$k^2(1-\gamma^2)\int_\Omega u^t(y)J_0(k|y|)\mathrm{d}S_y=4iA_0^*$$

If we consider small values of k, that is to say if we consider Rayleigh Scattering case, the following expansion are obtained :

$$\begin{cases} J_0(k|y|)=1+o(1) \\ A_0^*=\dfrac{i}{4}(-1+\gamma^2)k^2\pi R^2+o(k^2) \end{cases}$$

Moreover, if we assume that $u^t(y)$ has a limit (physically obvious), that gives us the following result for the circle (thanks to dominated convergence theorem and Ω bounded):

$$\Im\{\int_\Omega u^t(y)\mathrm{d}S_y\}\underset{|k|\to 0}{\to}0$$

Validity of the Code

The study of the case of the circle is a way to check the validity of the code. The solution is computed approached by a finite sum and is computed on the boundary of the inhomogeneity in the collocation points. The plot of both solutions (analytic and computed) is done (here $k=\frac{\pi}{3},\gamma=7,\theta=\arg(\vec{d})=\frac{\pi}{4}$) is shown in Fig. 3.1 and 3.2

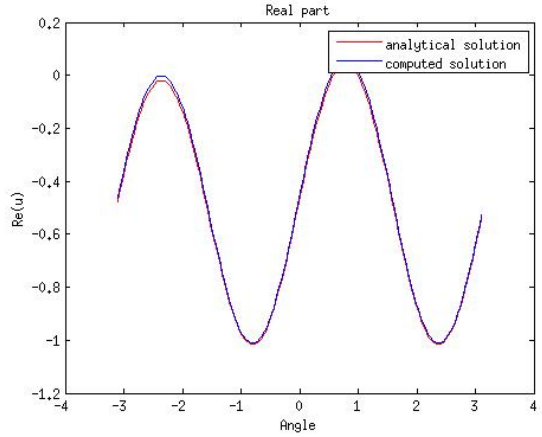

Figure 3.1: Real Part

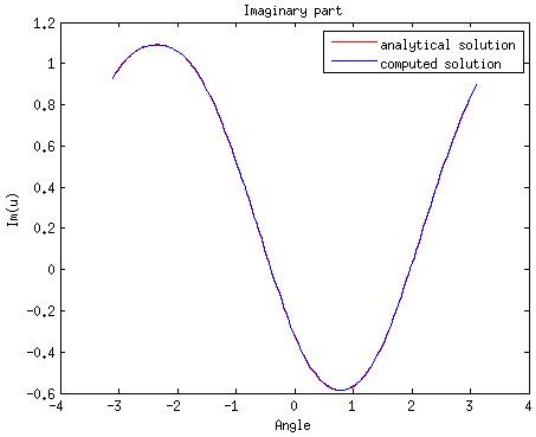

Figure 3.2: Imaginary Part

We can notice a very good match of both solutions.
Following the same idea, the integral of the imaginary part of the computed solution has to vanish when k goes to 0 , see figure 3.3 ($\gamma=0.7,\theta=\pi$).

The study of these two last results has been done in several test and configurations and the conclusion is still the same. Consequently, the validity of the code is established thanks to the case of one circular inclusion. Furthermore, results seem to be identical for a non circular inclusion, concerning the vanishment of the integral.

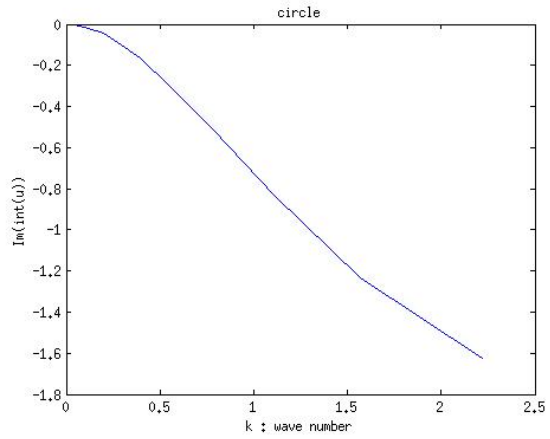

Figure 3.3: Imaginary Part of the integral for various values of k

3.2.2 Case of Non-circular and Multiple Inclusions

Now that the study is fully completed for the case of one circular inclusion. Now, our idea is to see how it works in the case of multiple and non circular inclusions.
For instance, it is interesting to see if the integral still vanishes when it is no longer a circle or a single inclusion.

Validity of the Code

Our main concern is to check if the case of multiple inclusions is valid too. For that purpose, it is useful to have an exact formula. Actually, in [4], there is one formula for two circular inclusions, in the case of Neumann problem ($\beta = 0$):
First, let us expand u^{inc} in two different manners (Jacobi-Anger):

$$\begin{cases} u^{inc} = \sum_m d_m^1 J_m(kr_1)e^{im\theta_1} = \sum_m d_m^2 J_m(kr_2)e^{im\theta_2} \\ d_m^j = i^m e^{-im\alpha} e^{ikb_j \cos(\mu_j - \alpha)} \end{cases}$$

where $\theta_1, \theta_2, r_1, r_2$ are defined in the figure 3.4 and $\alpha = \arg(\vec{d})$, $\mu_j = \arg(\vec{b_j})$, $\lambda = \arg(\vec{b})$ with $j = 1, 2$. Then, u^t is given by the following formula :

$$u^t = \sum_m \{d_m^1 J_m(kr_1) + c_m^1 H_m^1(kr_1) + \sum_n H_{m-n}^1(kb)e^{i(m-n)\lambda} c_n^2\} e^{im\theta_1}$$

where c_m^i for $i = 1, 2$ and $m \in \mathbb{Z}$ are solution of the following set of equations (a_i $i = 1, 2$ are the radii):

$$\begin{cases} c_m^1 H_m^{1\,\prime}(ka_1) + J_m'(ka_1) \sum_n H_{m-n}^1(kb)e^{i(m-n)\lambda} c_n^2 = -d_m^1 J_m'(ka_1) \\ c_m^2 H_m^{1\,\prime}(ka_2) + J_m'(ka_2) \sum_n H_{m-n}^1(kb)e^{i(m-n)(\pi-\lambda)} c_n^1 = -d_m^2 J_m'(ka_2) \end{cases}$$

For obvious technical reasons, m is in a finite set (for the tests, it was $[|-10, 10|]$). Consequently, the situation boils down to solve a linear system in the coefficients and then find the approached analytic solution. The computation has been in several cases, the figures 3.5 and 3.6 show us the results with $k = \pi, \gamma = \frac{1}{7}, \theta = \pi, \beta = 0.001$.

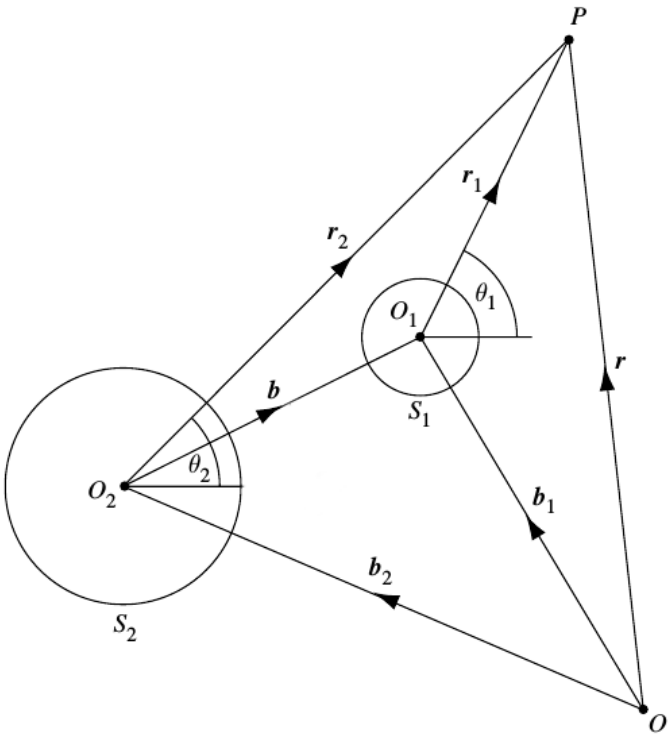

Figure 3.4: Notations for the case of two circles

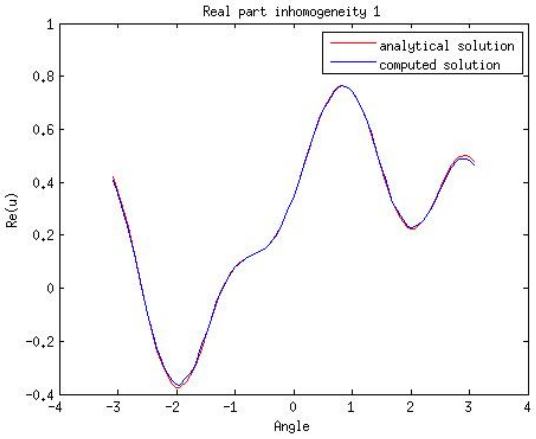

Figure 3.5: Real Part for the First Circle

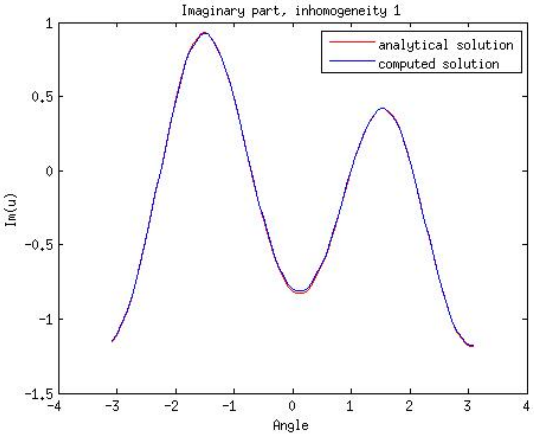

Figure 3.6: Imaginary Part for the First Circle

The corresponding geometry is shown in Fig. 3.7.

Curves obtained for the other inhomogeneity as well as for the other geometries are similar which leads us to the conclusion that the code is valid for the case of two circles and more generally for the case of multiple inclusions.

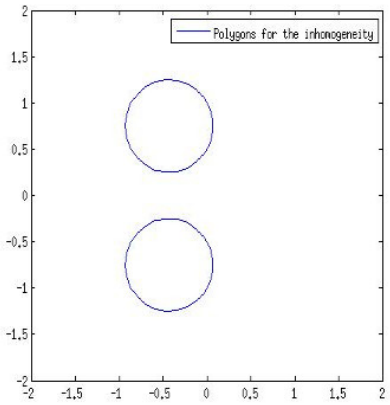

Figure 3.7: Geometry used for the case of two circles

3.2.3 Rayleigh Scattering

Now, in order to illustrate our assumptions about the behaviour of the integral for any type of inclusion, a low frequency or Rayleigh scattering analysis is done.
Based on the idea of the analysis in $\mathbb{R}^3$ made in [5], we can write :

$$u^{inc}(x) = \sum_{n=0}^{\infty} (ik)^n u_n^{inc}(x) \text{ where } u_n^{inc} = \frac{(\vec{d}.\vec{x})^n}{n!}$$

For small values of $k|x|$, we can assume that:

$$u^s(x) = \sum_{n=0}^{\infty} (ik)^n u_n^s(x) \text{ for } x \notin \Omega$$

where u_n^s is independent from k.
Thanks to Helmholtz equation in $\mathbb{R}^2 \setminus \Omega$, we immediately have:

$$\Delta u_0^s = \Delta u_1^s = 0$$

Since the expression of u_n^{inc} are known, we can find that :

$$\Delta u_0^{inc} = \Delta u_1^{inc} = \Delta u_0^t = \Delta u_1^t = 0$$

Based on the same idea, we can write that:

$$u^t(x) = \sum_{n=0}^{\infty} (ik)^n \gamma^n u_n^t(x) \text{ for } x \in \Omega$$

The transmission conditions give us:

$$\begin{cases} u_{n_+}^t = \gamma^n u_{n_-}^t \\ \dfrac{\partial u_n^t}{\partial n_+} = \gamma^n \dfrac{\partial u_n^t}{\partial n_-} \end{cases}$$

Thanks to Helmholtz equation we also have that:

$$\Delta u_0^t = \Delta u_1^t = 0$$

As it is explained in [5], we can prove that $u_0^t = 1$ in Ω and thanks to transmission condition and Laplace equation that $u_0^t = 1$ everywhere which means that $u_0^s = 0$. Consequently, when $k \to 0$

$$u^t(x) = 1 + O(k)$$

If we assume that $u^t(x)$ is regular enough and recall the independence to k of the other coefficients, it means that:

$$\begin{cases} \Re\{\int_\Omega u^t \mathrm{d}\Gamma\} = \mathcal{A}(\Omega) + O(k) \\ \Im\{\int_\Omega u^t \mathrm{d}\Gamma\} = O(k) \end{cases}$$

We can notice that thanks to these formulas, a generalization of the equations obtained with the circle has been found. Indeed, we have:

$$\begin{cases} (1-\gamma^2)\Re\{\int_\Omega u^t \mathrm{d}\Gamma\} = (1-\gamma^2)\pi R^2 + O(k) \\ \Im\{\int_\Omega u^t \mathrm{d}\Gamma\} = O(k) \end{cases}$$

Also, thanks to this expansion, we can have an expression of the far field pattern (since $e^{ik\hat{x}.y} = 1 + O(k)$)

$$u_\infty^s(x) = -k^2\{(1-\gamma^2)\mathcal{A}(\Omega)\} + O(k^3)$$

Finally, since we are still dealing with the case of $\beta = 1$, we can now equate the far field pattern of an inhomogeneity with its circular equivalent one for low frequencies:

$$(1-\gamma^2)\mathcal{A}(\Omega) = (1-\gamma_{eq}^2)\pi R_{eq}^2$$

Illustration with the Code

Thanks to this analysis, we can see that the vanishing of the imaginary part of the integral is independent from the shape of the inhomogeneity(ies). This can be illustrated via the diagrams shown in Fig. 3.8

Moreover, since the code is fully validated in the $\beta = 1$ case, we can have a correct view of the computed field. Here is the computed field with $\gamma = 0.7, k = \frac{\pi}{2}, \theta = \pi$:

The three inhomogeneities can be located due to the frequency change of the waves. Finally, thanks to the previous analysis, we are able to see what is the equivalent inhomogeneity in every case as long as the area of all the inhomogeneities is known. Let us do that in the case of 4 circles, for the same γ, the circular equivalent inhomogeneity can be a circle with a radius twice greater. In this case, since the far field pattern is real as well as for computed and analytic solutions, we only give the real part plot (figures 3.10 and 3.11).

Even if we can notice a difference between both curves (in figure 3.11), the shift (4.5×10^{-6}) is insignificant in comparison with the value of the field (1.52×10^{-3}). Moreover, the value is not exactly computed in the infinity, but really far from the origin.

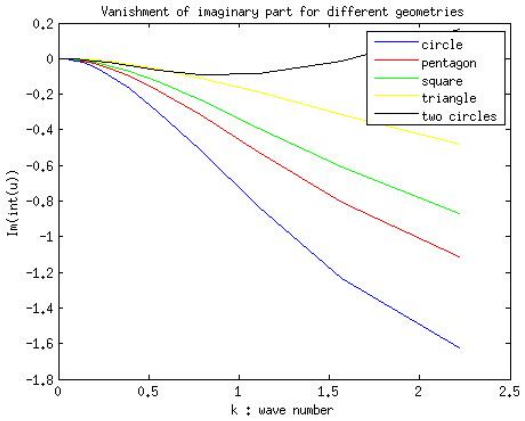

Figure 3.8: Imaginary Part of the integral for various values of k and diverse type of inclusions

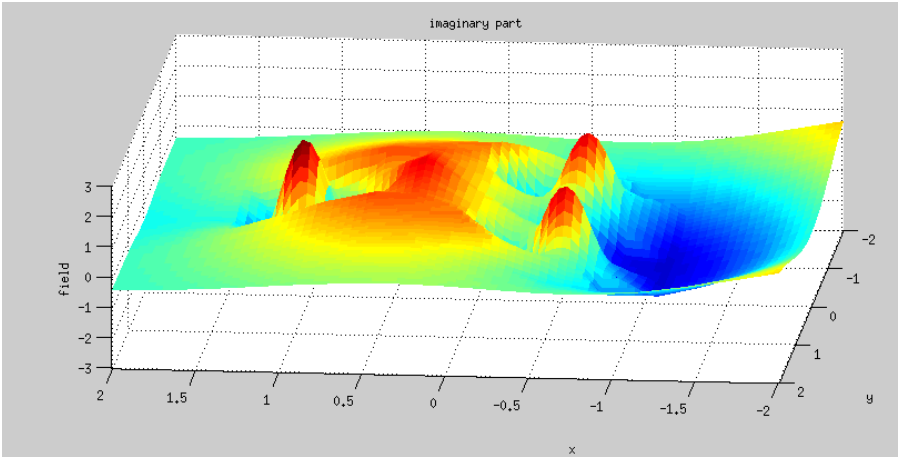

Figure 3.9: Computation of the imaginary part of the field with three circular inhomogeneities

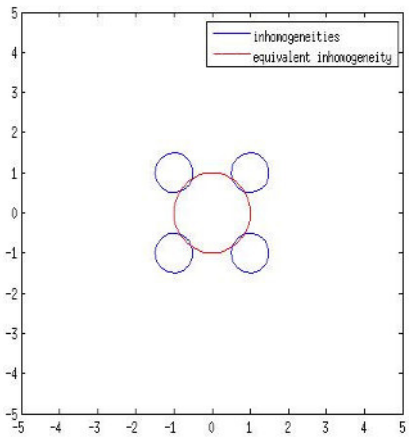

Figure 3.10: 4 circles and their circular equivalent inhomogeneity

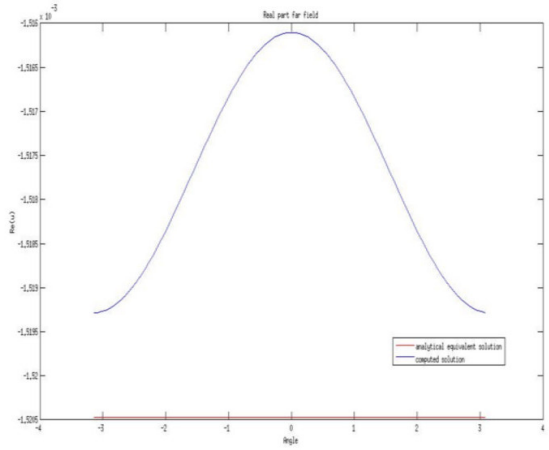

Figure 3.11: Far Field pattern generated by 4 circles and its circular equivalent one

3.3 Transmission Problem with $\beta \in \mathbb{R}$

Now, that $\beta \neq 1$, the analysis is not so simple. Physically, β is positive, but the study can be done without this assumption. A complete study of this case has been done in [2] (in 3D, but it can be done in 2D without loss of generality).
In short, the main outcome of this study is that we can reexpress the far field thanks to a static-study object : the polarization tensor $\mathbf{X}$. Consequently, the following far field pattern expansion is obtained for low frequencies:

$$u^s_\infty(\hat{x}) = -k^2\{(1-\beta\gamma^2)\mathcal{A}(\Omega) + (\hat{x})^\intercal \mathbf{X}(\beta)\vec{d}\} + O(k^3)$$

The polarization tensor has some properties:

$$\begin{cases} \mathbf{X}_{ij} = \mathbf{X}_{ij} \\ \dfrac{\beta-1}{\beta} < \dfrac{\mathbf{X}_{ii}}{\mathcal{A}(\Omega)} < \beta - 1 \\ (\mathbf{X}_{ij} - \dfrac{\beta-1}{\beta+1}\mathcal{A}(\Omega)\delta_{ij})^2 \leq (\mathbf{X}_{ii} - \dfrac{\beta-1}{\beta+1}\mathcal{A}(\Omega))(\mathbf{X}_{jj} - \dfrac{\beta-1}{\beta+1}\mathcal{A}(\Omega)) \end{cases}$$

In particular, this implies that $\mathbf{X} = 0$ when $\beta = 1$ which is in agreement with the formula obtained in the previous part.

Case of the Circle

Now let us have a look on the case of the circle. In that case, the polarization tensor has an explicit formula :

$$\mathbf{X} = 2\pi R^2 \frac{\beta-1}{\beta+1}\mathbf{I}_2$$

Which leads us to:

$$u^s_\infty(\hat{x}) = -k^2\{(1-\beta\gamma^2)\pi R^2 + 2\pi R^2 \frac{\beta-1}{\beta+1}\cos(\theta-\alpha)\} + O(k^3)$$

Actually, this formula can be obtained via another way. Indeed, if we start from the exact formula with any β:

$$u^s_\infty(\hat{x}) = \sum_{n=0}^{\infty} -4iA^*_n e^{-in\frac{\pi}{2}}\cos(n(\theta-\alpha))$$

with:

$$\begin{cases} A^*_n = ((-i)^n\epsilon_n)\dfrac{\beta\gamma J_n(kR)J'_n(\gamma kR) - J'_n(kR)J_n(\gamma kR)}{\beta\gamma H^1_n(kR)J'_n(\gamma kR) - H^{1\prime}_n(kR)J_n(\gamma kR)} \\ A^*_0 = \dfrac{i}{4}(-1+\beta\gamma^2)k^2\pi R^2 + O(k^3) \\ A^*_1 = \dfrac{\beta-1}{2(\beta+1)}k^2\pi R^2 + O(k^3) \\ A^*_n = O(k^{n+1}) \text{ for } n \geq 2 \end{cases}$$

Thanks to the last expansions, we find the same formula as previously.

Equivalent Inhomogeneity

Let us equate (for the first order) the far field pattern of an arbitrary set of inclusions to that of the equivalent inhomogeneity:

$$(1-\beta\gamma^2)\mathcal{A}(\Omega)+(\hat{x})^\intercal\mathbf{X}(\beta)\vec{d}=(1-\beta_{eq}{\gamma_{eq}}^2)\mathcal{A}(\Omega_{eq})+(\hat{x})^\intercal\mathbf{X_{eq}}(\beta_{eq})\vec{d}\quad\forall\vec{d},\hat{x}\in\mathbb{S}_2$$

Where $\mathbb{S}_2$ is the unit sphere of dimension 2. Let us integrate the previous equality for every $\vec{d}\in\mathbb{S}_2$:

$$\int_{\mathbb{S}_2}(1-\beta\gamma^2)\mathcal{A}(\Omega)+(\hat{x})^\intercal\mathbf{X}(\beta)\vec{d}\,\mathrm{d}S_{\vec{d}}=\int_{\mathbb{S}_2}(1-\beta_{eq}{\gamma_{eq}}^2)\mathcal{A}(\Omega_{eq})+(\hat{x})^\intercal\mathbf{X_{eq}}(\beta_{eq})\vec{d}\,\mathrm{d}S_{\vec{d}}$$

Since both $\mathbf{X},\hat{x}$ are independent of $\vec{d}$, we find

$$\int_{\mathbb{S}_2}(\hat{x})^\intercal\mathbf{X}(\beta)\vec{d}\,\mathrm{d}S_{\vec{d}}=(\hat{x})^\intercal\mathbf{X}(\beta)\{\int_{\mathbb{S}_2}\vec{d}\,\mathrm{d}S_{\vec{d}}\}=0\text{ since }\int_{\mathbb{S}_2}\vec{d}\,\mathrm{d}S_{\vec{d}}=0$$

Consequently, we obtain the following set of equations:

$$\begin{cases}(1-\beta\gamma^2)\mathcal{A}(\Omega)=(1-\beta_{eq}\gamma_{eq}^2)\mathcal{A}(\Omega_{eq})\\ \quad(\hat{x})^\intercal\mathbf{X}(\beta)\vec{d}=(\hat{x})^\intercal\mathbf{X_{eq}}(\beta_{eq})\vec{d}\quad\forall\hat{x},\vec{d}\in\mathbb{S}_2\end{cases}$$

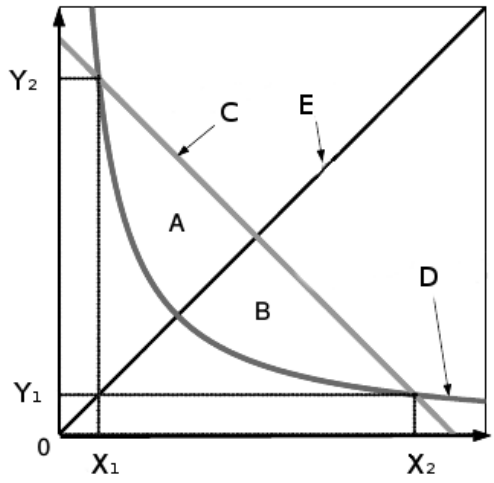

Figure 3.12: Wiener Box

Thanks to these two relations we can see to which extent, the idea of an equivalent inhomogeneity is valid or not. For that purpose, it is interesting to have a look on the properties of the polarization tensor and its eigenvalues (cf [6]):

- The polarization tensor is symmetric, positive definite if $\beta>1$ and negative definite if $\beta<1$
- If we denote κ_1 and κ_2 its two eigenvalues, we have the following optimal bounds (for $\beta>1$):

$$\begin{cases}\kappa_1+\kappa_2\leq\dfrac{(\beta-1)(\beta+1)}{\beta}\mathcal{A}(\Omega)\\ \dfrac{1}{\kappa_1}+\dfrac{1}{\kappa_2}\leq\dfrac{\beta+1}{(\beta-1)\mathcal{A}(\Omega)}\end{cases}$$

Thus, the eigenvalues are contained (for$\mathcal{A}(\Omega) = 1$) in the called *Wiener Box* in (κ_1, κ_2) space (see Fig. 3.12).
In Fig. 3.12, we have $X_1 = Y_1 = \frac{\beta-1}{\beta}$ and $X_2 = Y_2 = \beta - 1$. The curves C and D are respectively governed by the equations :

$$\begin{cases} \kappa_1 + \kappa_2 = \dfrac{(\beta-1)(\beta+1)}{\beta} \\ \dfrac{1}{\kappa_1} + \dfrac{1}{\kappa_2} = \dfrac{\beta+1}{(\beta-1)} \end{cases}$$

Starting from the intersection point of E and D, Fig. 3.13 give the evolution of the geometric shape of the inhomogeneity respectively along E.

Figure 3.13: Shape of the inhomogeneity along the curve E of 3.12

We are looking for an equivalent inhomogeneity, but it appears that only those cross-shaped domains, which are invariant under $\frac{\pi}{4}$ rotation, have a polarization tensor of form $\lambda\mathbf{I_2}$.
The main conclusion of this result, is that even in a first order approximation, we will never be able to find an exact circular equivalent inhomogeneity for an arbitrary set of inclusions.
Nevertheless, we can try to find the best approximation for an equivalent circular inhomogeneity. For that purpose, let us consider the following least squares problem:

$$\inf_{\lambda\in\mathbb{R}}\{\int_{\mathbb{S}_2\times\mathbb{S}_2} |(\hat{x})^\intercal(\mathbf{X}(\beta) - \lambda\mathbf{I_2})\vec{d}|^2 \, \mathrm{d}S_{\vec{d}} \, \mathrm{d}S_{\hat{x}}\}$$

Since $\mathbf{X}$ is real positive (or negative) define positive matrix, we know that it can be diagonalized in an orthonormal basis (made by its eigenvectors) with two eigenvalues strictly positives (or negatives) : κ_1, κ_2. Let us denote $\theta_1 = \arg(\hat{x})$ and $\theta_2 = \arg(\vec{d})$, the argument of these unit vector in this basis. Then, the formula can be rewritten as:

$$\inf_{\lambda\in\mathbb{R}} \frac{1}{4} \int_{\mathbb{S}_2\times\mathbb{S}_2} |(\frac{\kappa_1+\kappa_2}{2} - \lambda)\cos(\theta_1-\theta_2) + (\frac{\kappa_1-\kappa_2}{2})\cos(\theta_1+\theta_2)|^2 \, \mathrm{d}S_1 \, \mathrm{d}S_2$$

The solution of this quadratic optimization problem can be easily found. The functional is minimal when:

$$\lambda = \frac{\kappa_1+\kappa_2}{2}$$

If we recall that for a circle of radius R_{eq}, $\lambda = 2\pi R_{eq}^2 \frac{\beta_{eq}-1}{\beta_{eq}+1}$, we have a link between the eigenvalues of the inhomogeneity and the characteristics of the equivalent one. Moreover thanks to the inequalities involving the eigenvalues, we can have an approximation for numerical examples.

Equivalent Ellipse

The polarization tensor is actually known for an ellipse of great and small axis a and b:

$$\mathbf{X}(\beta) = \pi ab(\beta - 1) \begin{pmatrix} \frac{a+b}{a+\beta b} & 0 \\ 0 & \frac{a+b}{b+\beta a} \end{pmatrix}$$

If we recall, that for any polarization tensor, we can find an orthonormal basis in which it is diagonal and thus conclude that for any bunch of inclusion, we are able to find an equivalent whose far field pattern is the same as its.
Therefore, if we denote κ_1, κ_2 the eigenvalues of the related polarization tensor, the expression of a and b is given by:

$$\begin{cases} a = \sqrt{\dfrac{p}{\pi q}} \\ b = \sqrt{\dfrac{pq}{\pi}} \\ p = \dfrac{(\beta+1)(\kappa_1\kappa_2)}{(\beta-1)(\kappa_1+\kappa_2)} \\ q = \dfrac{\kappa_2 - \beta\kappa_1}{\kappa_1 - \beta\kappa_2} \end{cases}$$

Consequently, the problem is fully solved as long as we accept an elliptic equivalent inhomogeneity.

Simulations

The simulations are one way to find the equivalent inhomogeneity without having to diagonalize the matrix and find its eigenvalues.
Our first goal is to check the validity of our assumption for an equivalent circle according the least square approximation. In the limit case, we have the following approximations

$$\begin{cases} \lambda = \dfrac{\kappa_1 + \kappa_2}{2} \\ \kappa_1 + \kappa_2 = \dfrac{(\beta-1)(\beta+1)}{\beta}\mathcal{A}(\Omega) \end{cases} \text{ or } \begin{cases} \lambda = \dfrac{\kappa_1 + \kappa_2}{2} \\ \dfrac{1}{\kappa_1} + \dfrac{1}{\kappa_2} = \dfrac{\beta+1}{(\beta-1)\mathcal{A}(\Omega)} \end{cases}$$

Consequently, let us try :

$$\lambda_{upper} = \frac{(\beta-1)(\beta+1)\mathcal{A}(\Omega)}{2\beta} \text{ and } \lambda_{lower} = \frac{(\beta-1)\mathcal{A}(\Omega)}{2(\beta+1)}$$

Concerning the real part of the far field pattern, the results are respectively for 4 squared inhomogeneities and with $\beta = 5$ in Figs 3.15 and 3.14.
The plots give us the confirmation that between these two extreme cases, it is possible to obtain an equivalent circular inhomogeneity whose far-field is really close from the real one.

Now, we will check the availability of an exact equivalent elliptical inhomogeneity. Since the eigenvalues were unknowns, it was only a research via some experimentations. The first example (Figs 3.16 and 3.17) is still four squares but with a different incident wave. Even if it is not really clear on the figure, the equivalent inhomogeneity is not circular but an ellipse whose semi axes are 0.85 and 0.749. However we can see that in this case, a circular equivalent inhomogeneity is not unwise.

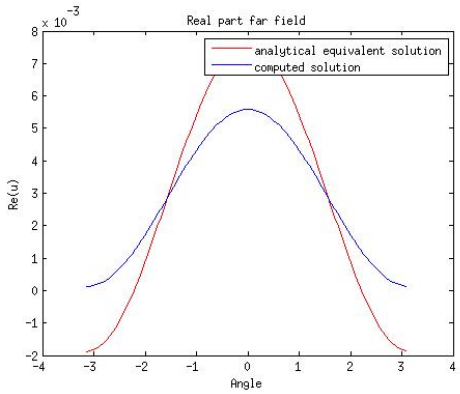

Figure 3.14: Far Field pattern generated by 4 squares and their circular equivalent inhomogeneity for the upper bound

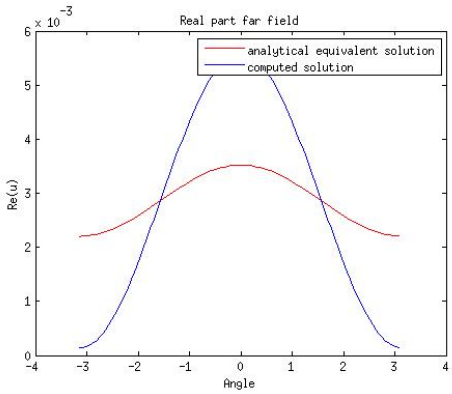

Figure 3.15: Far Field pattern generated by 4 squares and their circular equivalent inhomogeneity for the lower bound

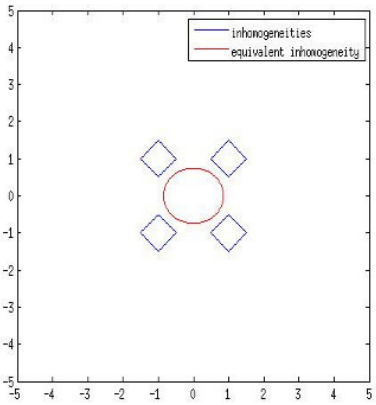

Figure 3.16: 4 squares and their elliptic equivalent inhomogeneity

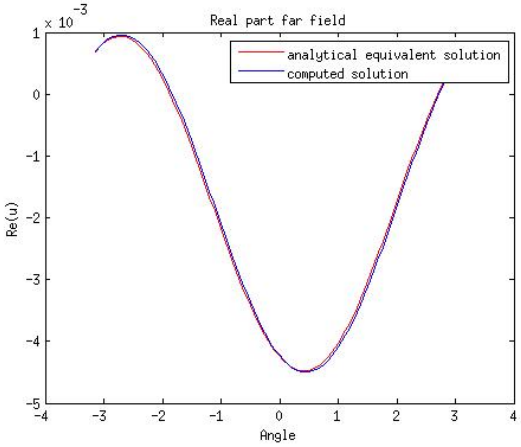

Figure 3.17: Far Field pattern generated by 4 squares and its elliptic equivalent one

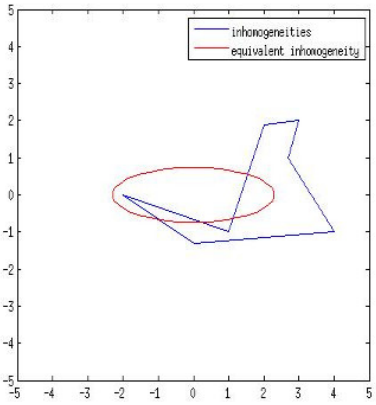

Figure 3.18: Random geometry and its elliptic equivalent inhomogeneity

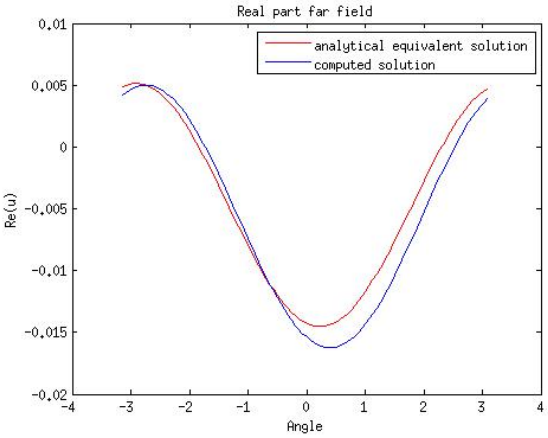

Figure 3.19: Far Field pattern generated by a random geometry and its elliptic equivalent one

The second example (figures 3.18 and 3.19) is a random geometry. We can notice that in this case, the elliptical equivalent inhomogeneity is not close at all from a circle. Moreover, some plots of the far-field pattern made with equivalent circular inhomogeneities show that a circle does not match for these cases.

3.4 Transmission Problem with Complex Parameters

Until now, we have only focused on real coefficients, as it is the case in acoustics and we noticed that this case has always been fully studied in a similar domain of electromagnetism and nothing really new has been brought. That is why the study with real coefficients is not as interesting as expected.
However, these coefficients can be complex, as it is the case with SH-waves in viscoelastics (in this case, γ is complex and β too, but $\frac{\beta}{\gamma^2}$ is real and for physical reasons, the imaginary part of both is positive) and this field seems to be totally new concerning homogenization problems. Hopefully, our asymptotic study remains the same whether our coefficients may be complex or not.

$$\begin{cases} (1-\beta\gamma^2)\mathcal{A}(\Omega) = (1-\beta_{eq}\gamma_{eq}^2)\mathcal{A}(\Omega_{eq}) \\ \qquad (\hat{x})^\intercal \mathbf{X}(\beta)\vec{d} = (\hat{x})^\intercal \mathbf{X_{eq}}(\beta_{eq})\vec{d} \quad \forall \hat{x}, \vec{d} \in \mathbb{S}_2 \end{cases}$$

We can notice that the expression of the polarization in the case of a circle and an ellipse remain the same. The polarization tensor is thus a complex symmetric matrix. In the general case this set of matrices has some non diagonalizable elements. However we can notice that the real and imaginary part are real symmetric matrices so that we can diagonalize them. What is actually missing is the link between these two matrices, for instance the link between their eigenvalues and eigenvectors.
If it turns out that the polarization tensor is diagonalizable even in the complex case, the thanks to the same reasoning as in the real case, we know that we can find an equivalent ellipse. But is it always the case ? Otherwise and that is the objective of the following explanations, we need to find some bounds for this tensor, so that we could conclude to the equivalent inhomogeneity in these limit cases.

Comparison with the Real Case

Nevertheless, we are at the moment not able to find the same relationship as in the real case with the eigenvalues of the real and the imaginary part. A very long study has been done on the real case papers (e.g. [6]) in order to see to which extent the work to obtain bounds could be generalized. If we want to understand the current problem, we have to focus on the main steps of the real case reasoning which are explained below.
First let us consider(with notations of [6]), the following static problem:

$$\begin{cases} \nabla.((1+(\beta-1)\chi(\Omega))\nabla u) = 0 \text{ in } \mathbb{R}^2 \\ u(x) - H(x) = O_{+\infty}(|x|^{-1}) \end{cases}$$

Where H is an harmonic function in $\mathbb{R}^2$ and is the equivalent of the free-field solution in our problem.

Let us denote the following functional operators for $\phi \in L^2(\Omega)$ (where $G(x-y)$ is the Green Function for the Laplacian):

$$\begin{cases} S_\Omega\phi(x) = \int\limits_{\partial\Omega} G(x-y)\phi(y)\mathrm{d}\Gamma_y \text{ for } x \in \mathbb{R}^2 \\ \kappa^*_\Omega\phi(x) = \dfrac{1}{\pi}\int\limits_{\partial\Omega} \dfrac{< x-y, n_x >}{|x-y|^2}\phi(y)\mathrm{d}\Gamma_y \end{cases}$$

Then, the solution is given by :

$$u(x) = H(x) + S_\Omega(\lambda I - \kappa^*_\Omega)^{-1}(\frac{\partial H}{\partial n}|_{\partial\Omega})(x)$$

where $\lambda = \frac{\beta+1}{2(\beta-1)}$.
The second term is the equivalent of the scattered field. This formula can be proved thanks to the jump relations (see Appendix) in $\partial\Omega$ governing these operators. Hence,

$$\begin{cases} (u-H)(x) = \displaystyle\sum_{|i|,|j|=1} \frac{(-1)^i}{i!j!}\partial^i_x G(x)\mathbf{X}_{ij}\partial^j H(0) \\ \mathbf{X}_{ij} = \displaystyle\int\limits_{\partial\Omega} y^j\phi_i(y)\mathrm{d}\Gamma_y \text{ for } i,j \in \mathbb{N}^2 \\ \phi_i(y) = (\lambda I - \kappa^*_\Omega)^{-1}(n_x.\nabla x^i)(y) \text{ for } y \in \partial\Omega \end{cases}$$

For $|i| = |j| = 1$, we have the first order polarization tensor, that is to say our subject of study. As said previously, the polarization tensor remains symmetric and the proof does not need to be changed.

The major step in the real case is the proof of the positive or negative definite character. Let us denote, for $a_1, a_2 \in \mathbb{R}$:

$$\begin{cases} f(y) = a_1y_1 + a_2y_2 \\ \phi(y) = a_1\phi_1 + a_2\phi_2 = (\lambda I - \kappa^*_\Omega)^{-1}(\dfrac{\partial f}{\partial n}) \end{cases}$$

It can be proved that:

$$\sum_{1\le i,j\le 2} a_ia_j\mathbf{X}_{ij} = \int\limits_{\partial\Omega} f\phi\mathrm{d}\Gamma = \frac{\beta-1}{\beta+1}\{\beta\int\limits_\Omega(\nabla(S_\Omega\phi+f))^2\mathrm{d}S + \int\limits_{\mathbb{R}^2\setminus\bar{\Omega}}(\nabla(S_\Omega\phi))^2\mathrm{d}S + \int\limits_\Omega(\nabla f)^2\mathrm{d}S\}$$

When β is real this relation is enough to prove the fact that $\mathbf{X}$ is positive (negative) definite.
At this point the equation are still true for the complex case, even if we cannot really use them. Our goal would be to obtain the same kind of *simple* relationship involving the real part and another the imaginary which would help to find if these matrices could be positive definite or not.

From this equation, we can also find the optimal bounds from the polarization tensor. Let us set $w_\Omega = S_\Omega\phi$, we have:

$$\begin{cases} \nabla.((1+(\beta-1)\chi(\Omega))\nabla(w_\Omega+f)) = 0 \text{ in } \mathbb{R}^2 \\ w_\Omega = O_{+\infty}(|x|^{-1}) \\ \displaystyle\int\limits_{\partial\Omega}\phi = 0 \end{cases}$$

All these equalities imply that $\forall v \in W$ where W is defined in the Appendix :

$$\int_{\mathbb{R}^2}(1+(\beta-1)\chi(\Omega))(\nabla w_\Omega+(1-\frac{1}{\beta})\chi(\Omega)\nabla f).\nabla v=0$$

That is an equivalent of an energy identity. In other words (**and complex coefficients case cannot go further in this analysis**), w_Ω is the minimizer of:

$$I_\Omega(w)=\int_{\mathbb{R}^2}(1+(\beta-1)\chi(\Omega))(\nabla w+(1-\frac{1}{\beta}))\chi(\Omega)\nabla f)^2$$

Taking the identity with $v=w_\Omega$:

$$-\int_{\mathbb{R}^2}(1+(\beta-1)\chi(\Omega))(\nabla w_\Omega)^2=(\beta-1)\int_\Omega \nabla f.\nabla w_\Omega$$

which yields:

$$\sum_{1\leq i,j\leq 2} a_i a_j \mathbf{X}_{ij}=I_\Omega(w_\Omega)+(1-\frac{1}{\beta})\int_\Omega(\nabla f)^2$$

This is the key identity to prove the optimal bounds. If we suppose that $\mathcal{A}(\Omega)=1$ and denote $a=(a_1,a_2)$,then:

$$\sum_{1\leq i,j\leq 2} a_i a_j \mathbf{X}_{ij}=\inf_{w\in W} I_\Omega(w)+(1-\frac{1}{\beta})\int_\Omega |a|^2$$

After that step, the idea in the real case is to apply the Hashin Shtrikman technique which is a well known variational technique that enables to obtain some optimal bounds on $\mathbf{X}$ when it satisfies this kind of equalities involving a functional minimization. The process is detailed in [6] and yields to:

$$\begin{cases} \mathrm{Tr}(\mathbf{X}) \leq \dfrac{(\beta-1)(\beta+1)}{\beta} \\ \mathrm{Tr}(\mathbf{X}^{-1}) \leq \dfrac{\beta+1}{\beta-1} \end{cases}$$

That is exactly the same equality with the trace instead of the eigenvalues.
Consequently, the idea for the complex case is to use the physical reasoning. Starting from the constitute equations of our problem, an equivalent of this energy identity could certainly be found. Thanks to these energy identities, we would be able to obtain some relationship of functional minimization on which we could apply the variational technique of Hashin Shtrikman. But the way has certainly to be different from the one of the real case, and it has not be found yet.

Some Ideas

- The case of complex matrices and variational principles has already been tackled in the case of conductivity problems (e.g in [7]).
  For instance, starting from the following constitutive relations (with all constituents complex):

$$\begin{cases} J=\sigma E \\ \nabla.J=0 \\ \nabla\times E=0 \end{cases}$$

Splitting real and imaginary part enables the relations to be changed in:

$$\begin{pmatrix} -J^{re} \\ J^{im} \end{pmatrix} = \begin{pmatrix} -\sigma^{re} & \sigma^{im} \\ \sigma^{im} & \sigma^{re} \end{pmatrix} \begin{pmatrix} E^{re} \\ E^{im} \end{pmatrix}$$

The idea, like it is explained in this paper, is to apply a variational principle to our matrix and its real and imaginary part. Nevertheless, if we want to apply such variational principle, we need to have a positive definite matrix. Consequently, the system is rewritten this way:

$$\begin{pmatrix} J^{im} \\ E^{im} \end{pmatrix} = \begin{pmatrix} \sigma^{im} + \sigma^{re}(\sigma^{im})^{-1}\sigma^{re} & \sigma^{re}(\sigma^{im})^{-1} \\ (\sigma^{im})^{-1}\sigma^{re} & \sigma^{im} \end{pmatrix} \begin{pmatrix} E^{re} \\ -J^{re} \end{pmatrix}$$

The matrix obtained is then positive definite as long as σ^{im} is. These are only assumptions, but if we succeed to find an equivalent of relatively simple constitutive relation and involving components of the polarization tensor, we would be able to apply this transformation and then obtain this matrix on which some variational principles can be applied.

- What we still can do is to find what is the best equivalent circular inhomogeneity regarding the least squares approximation. Since our set of equations for the equivalent inhomogeneity is still valid as well as the formula for the polarization tensor for a circle, the minimization problem reads:

$$\inf_{(\lambda_1,\lambda_2)\in\mathbb{R}^2} \int_{\mathbb{S}_2\times\mathbb{S}_2} \left|(\hat{x})^\intercal(\mathbf{X}(\beta) - (\lambda_1 + i\lambda_2)\mathbf{I_2})\vec{d}\right|^2 \, \mathrm{d}S_{\vec{d}} \, \mathrm{d}S_{\hat{x}}$$

Now let us write $\mathbf{X}(\beta) = \mathbf{X}_1(\beta) + i\mathbf{X}_2(\beta)$. We know that $\mathbf{X}_1(\beta)$ and $\mathbf{X}_2(\beta)$ are both real and symmetric matrices, which means that we can diagonalize them in an orthonormal basis. Let us denote (κ_1^1, κ_2^1) and (κ_1^2, κ_2^2) these eigenvalues, the minimization problem is consequently :

$$\begin{cases} \inf\limits_{(\lambda_1,\lambda_2)\in\mathbb{R}^2} \dfrac{1}{4}\{ \displaystyle\int_{\mathbb{S}_2\times\mathbb{S}_2} ((\frac{\kappa_1^1+\kappa_2^1}{2} - \lambda_1)\cos(\theta_1^1 - \theta_2^1) + (\frac{\kappa_1^1-\kappa_2^1}{2})\cos(\theta_1^1+\theta_2^1))^2 \, \mathrm{d}S_1^1 \, \mathrm{d}S_2^1 \\ \qquad + \displaystyle\int_{\mathbb{S}_2\times\mathbb{S}_2} ((\frac{\kappa_1^2+\kappa_2^2}{2} - \lambda_2)\cos(\theta_1^2 - \theta_2^2) + (\frac{\kappa_1^2-\kappa_2^2}{2})\cos(\theta_1^2+\theta_2^2))^2 \, \mathrm{d}S_1^2 \, \mathrm{d}S_2^2\} \end{cases}$$

This functional reaches its minimum when :

$$\begin{cases} \lambda_1 = \dfrac{\kappa_1^1 + \kappa_2^1}{2} \\ \lambda_2 = \dfrac{\kappa_1^2 + \kappa_2^2}{2} \end{cases}$$

If we recall that for a circle of radius R_{eq} $\lambda = \lambda_1 + i\lambda_2 = 2\pi R_{eq}^2 \frac{\beta_{eq}-1}{\beta_{eq}+1}$, a link is established between the best circular equivalent inhomogeneity in the sense of the least square and the eigenvalues of the real ad the imaginary part. But in contrast to the real case, we don't have at the time neither the other relationship nor inequality concerning these eigenvalues.

Some Tests with the Code

The first step is to check the validity of our exact formulas in the case of the circle in order to be sure that the expansion is still true for complex coefficients and that the code still works. Consequently, let us plot the far field pattern for both real and imaginary part for one circle wit the following parameters : $\gamma = 0.7(1 + 0.5i), \beta = 5\gamma^2, \theta = \frac{\pi}{7}, k = \frac{\pi}{100}$ (needed to analyze far-field pattern):

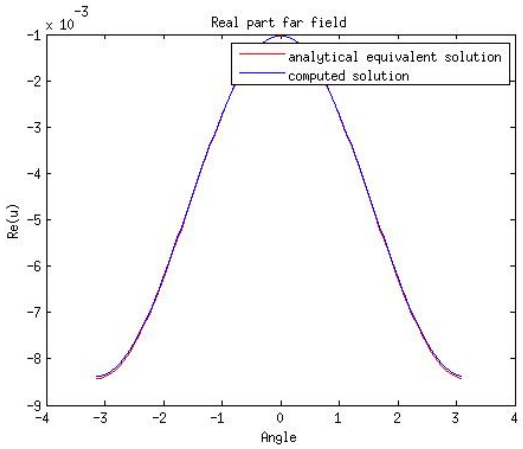

Figure 3.20: Real part of the far Field pattern generated by a circle compared with theoretical formula

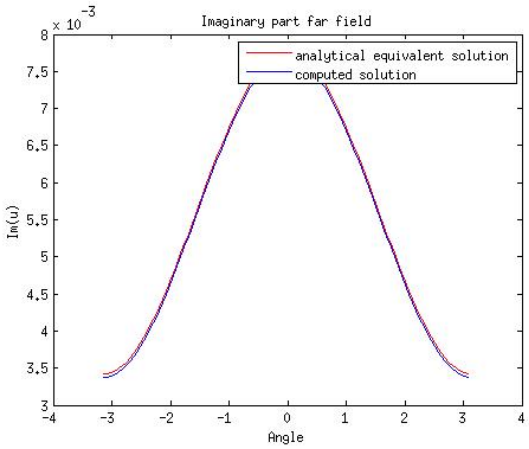

Figure 3.21: Imaginary part of the far Field pattern generated by a circle compared with theoretical formula

We can notice that the formula matches perfectly for the case of the circle which confirms us the idea that the assumption about the expansion and the exact formulas are still valid when it comes to complex coefficients.
Now, we have to see if the formulas found for the equivalent inhomogeneity still hold true. For that purpose, let us take again the case of 4 circles with their circular equivalent inhomogeneity (Figs. 3.22 and 3.23).
In the same way as in the case of the circle, we can see a perfect match of both curves in the plot.
Nonetheless, the theoretical study is relatively limited in this case, that is why we cannot look for an equivalent ellipse or geometry for the other cases. We tried to compare the fields found in the previous part for the equivalent ellipse for the four squares and the random geometry, but the curves do not match at all. In the same way, we don't have any bound to see if we can have an ellipse according to the least squares approximation. The apparition of complex coefficient certainly changes the behaviour of the equivalent inhomogeneity. It might be possible that an equivalent elliptic inhomogeneity may exist, but at the time, we are not able to prove it, neither theoretically nor numerically (for the tested configurations).

At least, this study gives us the opportunity to have a view of the field generated by the inhomogeneities. Here are the plots with the same parameters as previously except $k = \frac{\pi}{2}$, provided as an example.

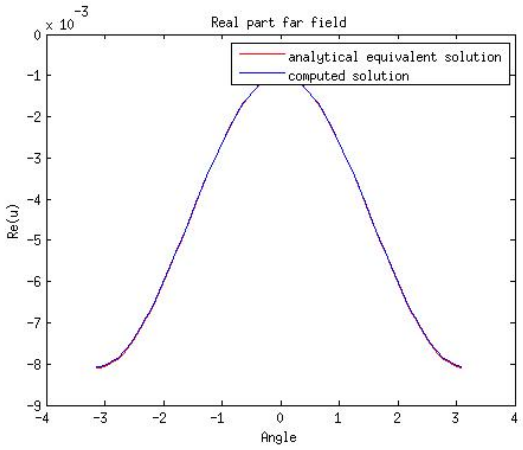

Figure 3.22: Real part of the far Field pattern generated by 4 circles compared with their circular equivalent inhomogeneity

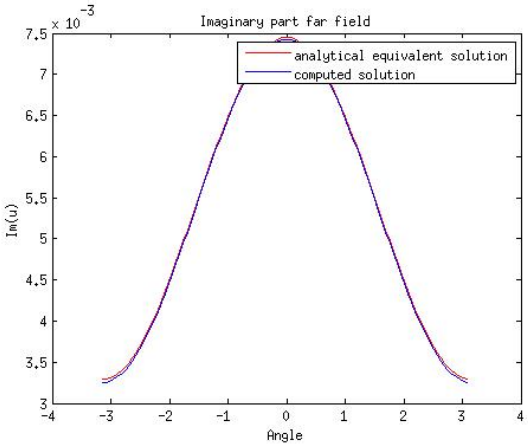

Figure 3.23: Imaginary part of the far Field pattern generated by 4 circles compared with their circular equivalent inhomogeneity

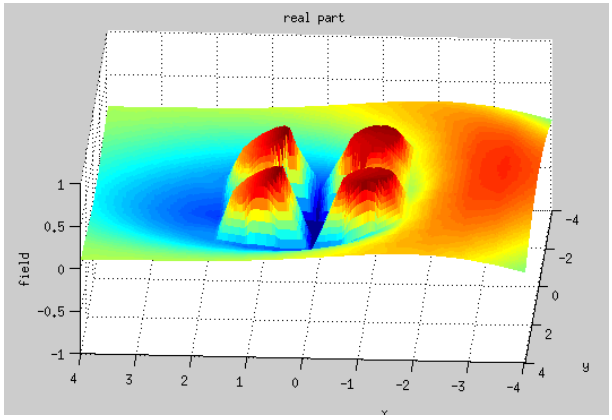

Figure 3.24: Real part of the Field generated by 4 circles

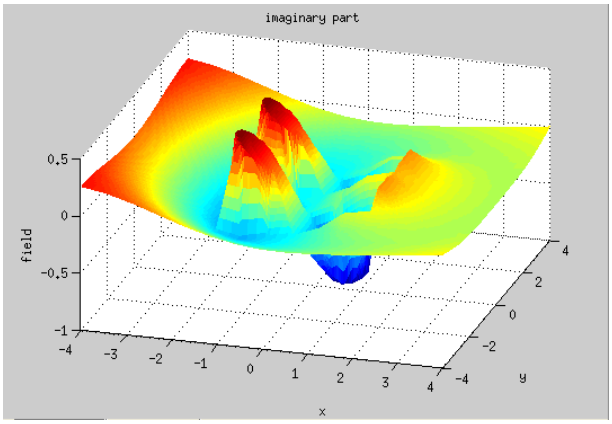

Figure 3.25: Imaginary part of the Field generated by 4 circles

3.5 Comments on the Theoretical Study

This part which was the guideline of the whole internship (and even in the end the only work to do) was actually the less efficient part of the internship. Indeed, this field of research was new to everybody : my supervisors and I.
Consequently, we had to do a literature survey. This literature survey and more especially the study of [6] was really tough. It was a good deal of abstract mathematical considerations and it was difficult to see the equivalent with our more physical/mechanical problem. Sometimes the results can be disappointing. For instance, the results of the far-field analysis in the case $\beta = 1$ were really disappointing because they are really simple, the polarization tensor is 0.
On an equal foot, the results of the real case were too. We were expecting to be on something new, but we discovered [6] which was in the same time a great help and forced us to see another cases, like viscoelastics. But, as it was said to me, "that's research !".

Conclusion

This internship has been a rich and interesting experience in different ways:
It was the opportunity to discover a new way to discretize partial differential equation and to implement it with MatLab. I was personally amazed by the efficiency and the accuracy of this code with a small number of points. That was the first time I entirely had to implement a simulation code.

It has been the possiblity to see how research on references is done ,how to interpret it and especially how to adapt it for our own research project. This has been too the possibility to be under a real research process which includes to work for weeks on some work that would probably never be reused afterwards.
This subject has evolved from the beginning. The first purpose was to study this in the acoustics case (i.e. when β is real), but it turned out that the case was mostly tackled in similar cases, that is why it was decided to focus on viscoelastics (i.e. when β is complex).This research is only at its beginning and certainly that most of the outcome will be in viscoelastics waves study, but the code will be used for this project and is almost completed even if it can be improved. The research team is very optimistic about finding something but it will need time and maybe other approaches that have not been found or tested yet.

To conclude, this research project could lead to some applications, for instance in medical imaging, where the viscoelastics model is used to detect tumors in a human organism.

Bibliography

[1] Marc Bonnet. *Boundary Integral Equations Methods for Solids and Fluids.* Wiley, 1999.

[2] Milton Abramowitz and Irene A. Stegun. *Handbook of Mathematical Functions With Formulas, Graphs, and Mathematical Tables.* U.S. Department of Commerce, 1964.

[3] A. Cemal Eringen and Erdogan S. Suhubi. *Elastodynamics: Linear Theory v. 2.* Academic Press, 1975.

[4] P.A. Martin. *Multiple Scattering.* Cambridge University Press, 2006.

[5] R.E Kleinman and T.B.A Senior. *Low and High frequency asymptotics.* Elsevier Science Publishers B.V., 1986.

[6] H. Ammari and H. Kang. *Polarization and Moment Tensors.* Springer, 2007.

[7] Russel Bingham Richins. *Some applications of minimizing variational principles for the complex Helmholtz equation.* Univerity of Utah, 2010.

Appendix

Jump Relations for Integral Operators

The integral operators mentioned in part 3.4 are ruled by the following jump relations on the boundary:

$$\begin{cases} S_\Omega\phi|_+(x) = S_\Omega\phi|_-(x) \\ \dfrac{\partial}{\partial n}S_\Omega\phi|_\pm(x) = (\pm\dfrac{1}{2}I + \kappa_\Omega^*)\phi(x) \qquad \forall x \in \partial\Omega \\ \dfrac{\partial}{\partial n}S_\Omega\phi|_+(x) = \dfrac{\partial}{\partial n}S_\Omega\phi|_-(x) + \phi(x) \end{cases}$$

Definition of the space W

$$W = \left\{ w \in H^1_{loc}(\mathbb{R}^2) : \frac{w}{\sqrt{1+|x|^2}\ln(2+|x|^2)} \in L^2(\mathbb{R}^2), \nabla w \in L^2(\mathbb{R}^2) \right\}$$

This space is constructed so that Δ can set an isomorphism between W and its dual. This property is useful to prove the optimal bounds in the real case. For further explanations, see [6]